Desalination and Water Treatment
www.deswater.com

doi: 10.1080/19443994.2015.1038595

57 (2016) 10515–10522
May

Taylor & Francis
Taylor & Francis Group

CFD simulation of water transport through porous membrane evaporators

Mehrnoush Mohammadi[a,*], Seyyed Masoud Kazemi[b], Rezvan Torkaman[c]

[a]*Faculty of Engineering, Department of Chemical Engineering, South Tehran Branch, Islamic Azad University, P.O. Box 11365-4435, Tehran, Iran, Tel. +98 21 33722831; Fax: +98 21 66051553; email: mehrnoush_mohammadi@yahoo.com*
[b]*Faculty of Chemistry, Department of Analytical Chemistry, North Tehran Branch, Islamic Azad University, Tehran, Iran, email: masoudkazemi1394@gmail.com*
[c]*Nuclear Fuel Cycle Research School, Nuclear Science and Technology Research Institute, P.O. Box 14155-1339, Tehran, Iran, email: r.torkaman@alumni.ut.ac.ir*

Received 30 January 2015; Accepted 30 March 2015

ABSTRACT

Membrane evaporation (ME) presents interesting working conditions including low operating temperature and also low energy consumption. These advantages make the process attractive for concentration of aqueous solutions containing heat-sensitive components. Performance of ME process carried out in a flat-sheet membrane contactor was studied theoretically in this work. A three-dimensional mathematical model was developed to predict the performance of ME process. The concentration, momentum, and energy equations were solved for description of process. Finite element method was utilized for solution of governing equations and simulation of process. By obtaining the concentration distribution, the flux of water evaporation was determined and compared with the experimental data reported in literature. It was also indicated that the developed three-dimensional model is appropriate for the prediction of the performance of membrane evaporators. The simulation results revealed that enhancement of velocity of liquid phase increases evaporation flux of water.

Keywords: Membrane; Computational fluid dynamics; Numerical simulation; Mass transfer; Evaporator

1. Introduction

During the past years, membrane technology has shown great ability in concentration of aqueous solutions. Membrane technology is more attractive when a heat-sensitive solution needs to be treated. In the latter case, conventional processes such as distillation or evaporation cannot be utilized due to processing at high temperature. Another important restriction of conventional processes for concentration of aqueous solutions is consumption of much energy which in turn results in enhancement of process costs and also environmental problems [1,2].

Membrane processes that can be used for concentration of aqueous solutions include osmotic evaporation (OE), membrane distillation (MD), and membrane evaporation (ME) [3,4]. Among these processes, ME is a novel process which is halfway between OE and MD. This process represents advantages of concentration processes and can be considered as a promising technology for concentration of aqueous solutions. ME process is based on the application of a hydrophobic

*Corresponding author.

macroporous or mesoporous membrane which separates an aqueous solution to be concentrated and a stripping phase. The stripping phase is a low pressure gas, which is mostly dry air. The basic principle of ME is illustrated in Fig. 1 [5,6].

It should be pointed out that on the contrary to MD and OE, in ME, the flow of water vapor is not condensed, but it is taken away by the stripping phase (air).

ME operates at room temperature, and the driving force of the process is not the thermal gradient, but the difference of the partial pressure of vapor between water surface and dry air. ME thus represents interesting working conditions, and most particularly low operating temperature. The latter makes this process attractive for heat-sensitive solutions [4,7–9].

A few studies have been conducted on modeling of mass transfer in ME process [4,7–10]. A comprehensive mathematical model was developed for the prediction of water evaporation in ME by Hengl et al. [4]. The model was based on resistance in-series which considered two mass transfer resistances, i.e. membrane and gas phase [5,6].

Another study was conducted by Mourgues et al. [10]. They also used resistance-in-series model to predict the mass and heat transfer in the ME. The objective of their modeling was to optimize ME by determining the main resistances to the transfer as well as estimating the evaporating flux evolution vs. the operating conditions and membrane structure.

The main purpose of this study was to develop and solve a mass transfer model for description of ME. Computational fluid dynamics (CFD) technique is used to solve the model equations. The model findings are then validated through comparing with experimental data reported in literature.

2. Theory

Fig. 2 indicates the domain used for development of mathematical model. As it can be seen from Fig. 2, the model domain comprises three parts, i.e. liquid phase including pure water, porous membrane, and gas phase containing air. The model equations are developed for these parts.

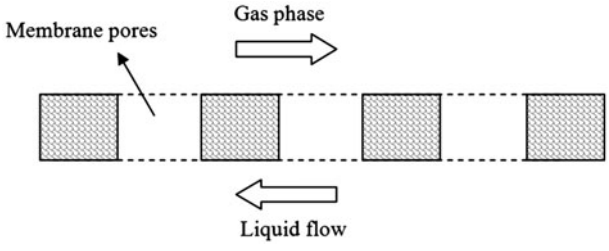

Fig. 1. Basic principle of ME.

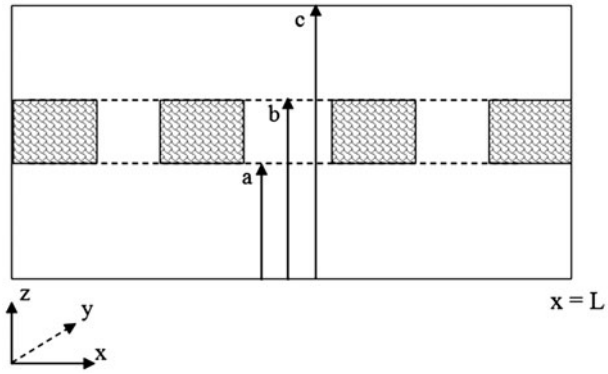

Fig. 2. Model domain.

2.1. Gas phase

The continuity equation is used for prediction of water vapor concentration in the gas phase [11]:

$$D_{\mathrm{w-air}}\left[\frac{\partial^2 C_{\mathrm{w-gas}}}{\partial x^2}+\frac{\partial^2 C_{\mathrm{w-gas}}}{\partial y^2}+\frac{\partial^2 C_{\mathrm{w-gas}}}{\partial z^2}\right] = V_{x-\mathrm{g}}\frac{\partial C_{\mathrm{w-gas}}}{\partial x} \tag{1}$$

where $V_{x-\mathrm{g}}$ refers to the velocity of gas phase in x-direction. The Navier–Stokes equations are used to determine the velocity distribution in the gas phase [6]:

$$-\nabla\cdot\eta_{\mathrm{g}}\left(\nabla V_{x-\mathrm{g}}+(\nabla V_{x-\mathrm{g}})^{T}\right)+\rho_{\mathrm{g}}\left(V_{x-\mathrm{g}}\cdot\nabla\right)V_{x-\mathrm{g}}+\nabla p_{\mathrm{g}} = F_{\mathrm{g}}\nabla\cdot V_{x-\mathrm{g}} = 0 \tag{2}$$

The boundary conditions for the gas phase may be written as follows:

$$@\ x = 0;\quad C_{\mathrm{w-gas}} = C_0 \tag{3}$$

$$@\ x = L;\quad \text{Convective flux} \tag{4}$$

$$@\ z = b;\quad C_{\mathrm{w-gas}} = C_{\mathrm{w-membrane}} \tag{5}$$

$$@\ z = c;\quad \frac{\partial C_{\mathrm{w-gas}}}{\partial z} = 0 \tag{6}$$

$$@\ y = 0\ \&\ y = w; \quad \frac{\partial C_{w-gas}}{\partial y} = 0 \tag{7}$$

The boundary condition "convective flux" applied in Eq. (4) assumes that mass transfer through this boundary is convectivedominated, and the contribution of diffusion is negligible.

Boundary conditions for the Navier–stokes equations may be written as follows:

$$@\ x = 0; \quad V_{x-g} = V_0 \tag{8}$$

$$@\ x = L; \quad p = p_{atm} \tag{9}$$

$$@\ z = b; \quad V_{x-g} = 0 \tag{10}$$

$$@\ z = c; \quad V_{x-g} = 0 \tag{11}$$

$$@\ y = 0\ \&\ y = w; \quad V_{x-g} = 0 \tag{12}$$

2.2. Equations of membrane

The concentration of water vapor inside the membrane pores is determined using solution of mass transfer equation:

$$D_{w-membrane}\left[\frac{\partial^2 C_{w-membrane}}{\partial x^2} + \frac{\partial^2 C_{w-membrane}}{\partial y^2} + \frac{\partial^2 C_{w-membrane}}{\partial z^2}\right] = 0 \tag{13}$$

where $D_{w-membrane}$ refers to effective diffusion coefficient of water vapor inside the membrane which is calculated using the porosity and tortuosity of the membrane [12]:

$$D_{w-membrane} = D_{w-air}\left(\frac{\varepsilon}{\tau}\right) \tag{14}$$

The boundary conditions for the membrane may be written as follows:

$$@\ x = 0\ \&\ x = L; \quad \frac{\partial C_{w-membrane}}{\partial x} = 0 \tag{15}$$

$$@\ z = b; \quad C_{w-membrane} = C_{w-gas} \tag{16}$$

$$@\ z = a; \quad C_{w-membrane} = \frac{P_w^{sat}}{RT} \tag{17}$$

$$@\ y = 0\ \&\ y = w; \quad \frac{\partial C_{w-membrane}}{\partial y} = 0 \tag{18}$$

where L refers to the length of membrane, and P_w^{sat} is vapor pressure of saturated water at the membrane–water interface.

The equation for the heat conduction within the membrane is written as follows:

$$k\left[\frac{\partial^2 T_m}{\partial x^2} + \frac{\partial^2 T_m}{\partial y^2} + \frac{\partial^2 T_m}{\partial z^2}\right] = 0 \tag{19}$$

where k refers to the overall heat conductivity. It should be noted that heat conductivity through the membrane is calculated as the sum of two parallel heat transfer resistances, i.e. the heat conductivity through the solid part and the heat conductivity through the pores filled with gas and vapor [6]. The boundary conditions for heat transfer through the membrane are as follows:

$$@\ x = 0\ \&\ x = L; \quad \frac{\partial T_m}{\partial x} = 0 \tag{20}$$

$$@\ y = 0\ \&\ y = w; \quad \frac{\partial T_m}{\partial y} = 0 \tag{21}$$

$$@\ z = a; \quad T_m = T_w \tag{22}$$

$$@\ z = b; \quad T_m = T_g \tag{23}$$

2.3. Equations of liquid phase

In the liquid side, pure water is flown, and therefore, the concentration equation is not solved for this subdomain. The energy equation should be solved for the liquid phase to calculate the temperature distribution in this subdomain. Energy equation for the liquid phase may be written as [11] follows:

$$k_w\left[\frac{\partial^2 T_w}{\partial x^2} + \frac{\partial^2 T_w}{\partial y^2} + \frac{\partial^2 T_w}{\partial z^2}\right] = \rho_w C_{p-w} V_{x-w} \frac{\partial T_w}{\partial x} \tag{24}$$

where V_{x-w} refers to the velocity of water in the x-direction in liquid phase. The velocity distribution in liquid phase is calculated using the Navier–Stokes equations:

$$-\nabla \cdot \eta_w\left(\nabla V_{x-w} + (\nabla V_{x-w})^T\right) + \rho_w\left(V_{x-w} \cdot \nabla\right)V_{x-w} + \nabla p_w = F_w \nabla \cdot V_{x-w} = 0 \tag{25}$$

The boundary conditions for the energy equation are as follows:

$$@\ x = L; \quad T_w = T_0 \tag{26}$$

$$@\ x = 0; \quad \text{convective flux} \tag{27}$$

$$@\ z = 0; \quad \frac{\partial T_w}{\partial z} = 0 \tag{28}$$

$$@\ z = a; \quad q = N_w \Delta H_w \tag{29}$$

$$@\ y = 0\ \&\ y = w; \quad \frac{\partial T_w}{\partial y} = 0 \tag{30}$$

2.4. Numerical solution of model equations

The governing equations for all parts of system with boundary conditions were solved numerically using COMSOL Multiphysics software. The accuracy of the software and its numerical solvers in simulation of membrane processes have been proved by a number of previous authors [13–24]. To solve the set of equations, the finite element analysis is combined with adaptive meshing and error control using numerical solver of UMFPACK which is appropriate for these processes [16,25–35]. An IBM-PC-Pentium5 (CPU speed of 2,600 MHz and 2 GB of RAM) was used to solve the set of equations. The computational time for solving the set of equations was about 5 min. It should be pointed out that the COMSOL mesh generator creates triangular meshes which are isotropic in size.

Table 1
Parameters used in the numerical simulations

Membrane material	Stainless steel
Membrane length (mm)	210
Membrane width (mm)	127
Membrane thickness (mm)	0.2
Membrane porosity	0.3
Mean pore diameter (μm)	2.6
Water side height (mm)	5
Gas side height (mm)	15
Liquid temperature (K)	298.15
Gas temperature (K)	293.15

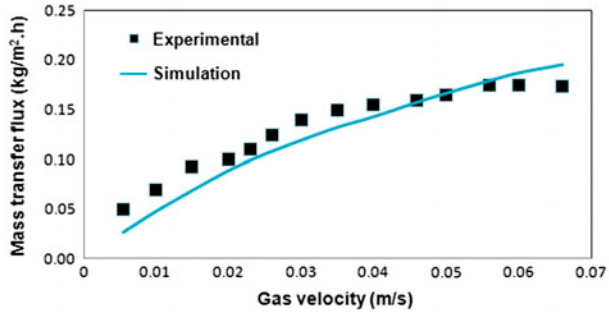

Fig. 3. Comparisons between experimental data and model predictions.

A large number of elements are then created with scaling. Different scaling factors have been employed in all directions due to large differences among

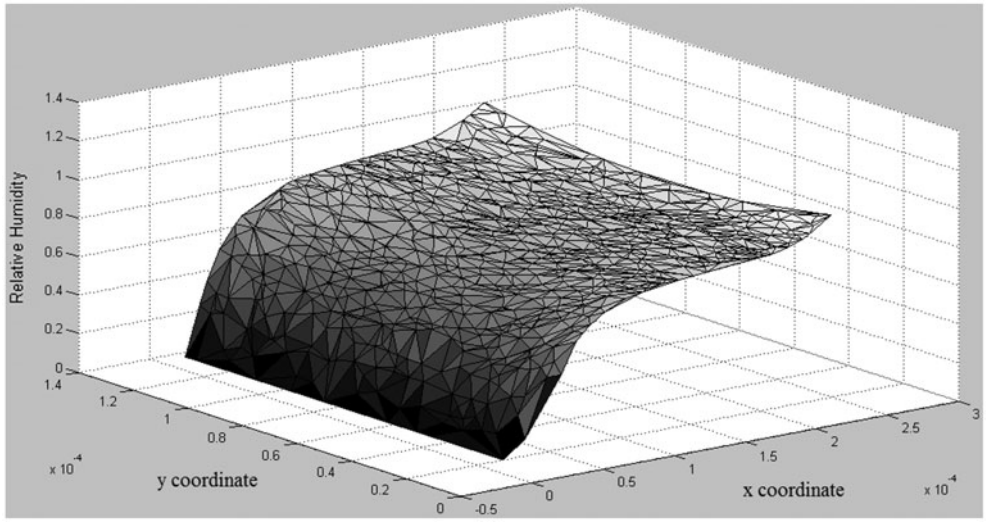

Fig. 4. Concentration distribution of water vapor in the gas phase; gas velocity = 0.066 m/s; water velocity = 0.0136 m/s; air inlet relative humidity = 0.07.

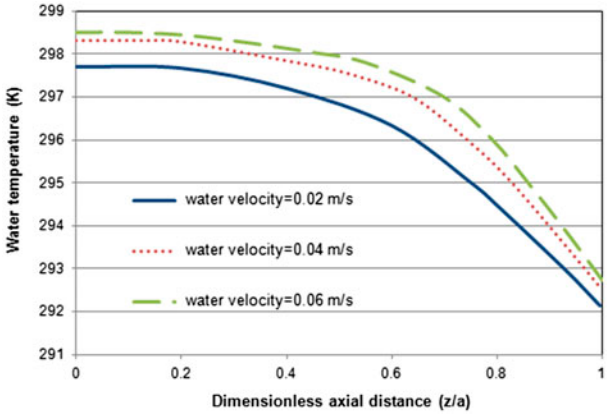

Fig. 5. Temperature profile of water in z-direction for different values of liquid velocity.

dimensions. This would generate an anisotropic mesh around 10,064 elements [6]. The membrane parameters used in the simulations are the same as those reported by Hengl et al. [4] and are listed in Table 1.

3. Results and discussion

3.1. Model validation

The model findings were compared with the experimental results reported by Hengl et al. [4] to validate the model and numerical procedure developed in this study. The results of comparison are shown in Fig. 3. Mass transfer flux of water vapor was chosen as the most important parameter for comparisons. As it is seen, the results of simulation are in good agreement with the experimental data. The model can predict the performance of ME process well at various velocity of gas phase. The velocity of air in the gas side increases from 0.005 to 0.066 m/s, while the mass transfer flux of water vapor increases up to 0.2 kg/m^2 h.

3.2. Concentration of water vapor in the gas phase

Fig. 4 illustrates concentration distribution of water vapor in the gas phase. The concentration is shown in terms of relative humidity. It is clearly shown that concentration of water vapor in the gas phase increases along the length of gas side in membrane module (x-direction). At the inlet of gas phase, the concentration of water vapor (humidity) is zero which implies the dry air at the entrance of membrane module. As the air moves in the gas side, water vapor is transferred to the air which in turn increases the humidity of air. It is also seen that at the outlet of gas phase, the relative humidity of air is near 1 which implies the saturation of air with water vapor during the process.

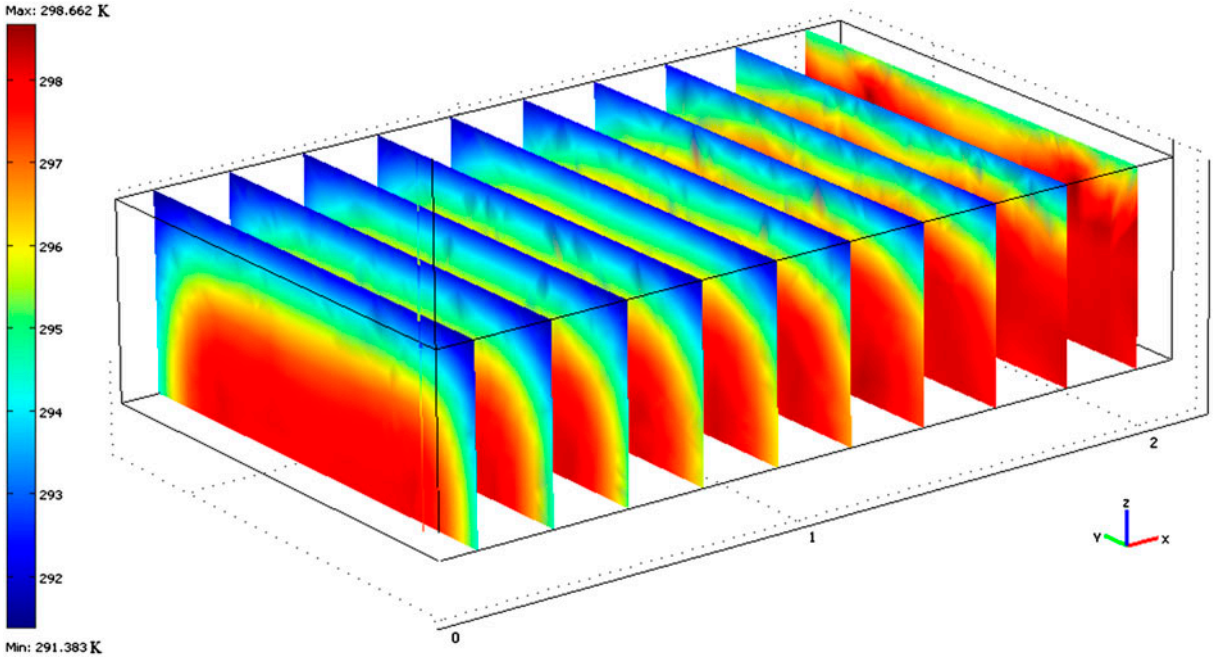

Fig. 6. Slices of water temperature distribution in the liquid side of the membrane evaporator; water velocity = 0.02 m/s.

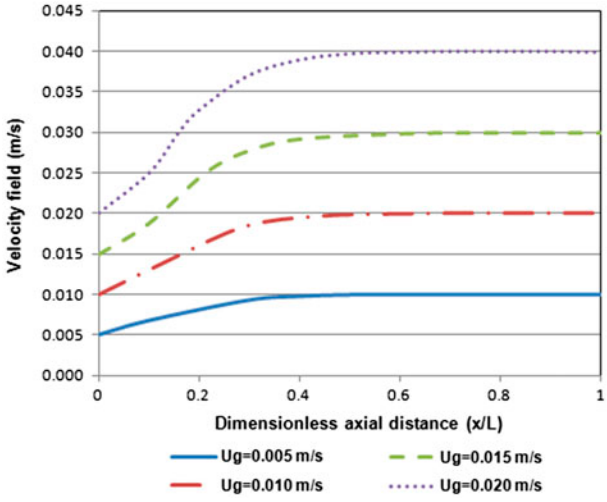

Fig. 7. Profile of velocity in the gas phase of membrane evaporator.

3.3. Temperature distribution in the liquid phase

Variations of liquid-phase temperature in the z-direction are shown in Fig. 5. Since the evaporation process is endothermic, the water gets cooled when it is evaporated into the air. It is also seen that variation of water temperature is sharper at the region near the membrane wall which reveals the formation of boundary layer in this region. Fig. 6 also exhibits temperature variations in the water side of the membrane module as slices in three dimensions. Identification of temperature drop would assist in predicting the performance of ME process accurately.

3.4. Velocity profile in the gas phase

Velocity profile in the gas phase of membrane evaporator is shown in Fig. 7, in which the air flows.

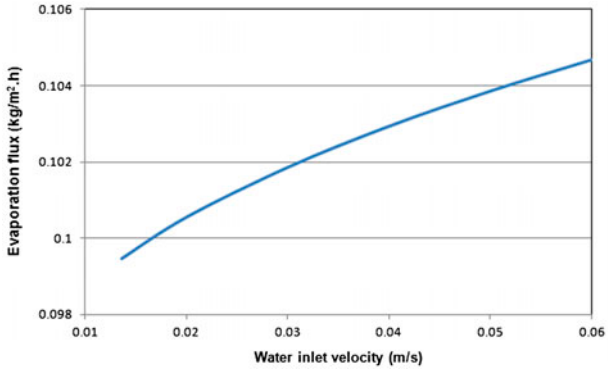

Fig. 8. Effect of water inlet velocity on evaporation flux.

The velocity profile in the gas phase side was determined by solving Navier–Stokes equations. As it can be seen from Fig. 7, velocity profile is not fully developed at the regions near the inlet of gas phase. As the gas flows through the gas side, the velocity tends to fully develop. Fig. 7 indicates that for different gas velocities, velocity reaches fully developed at almost middle of the membrane module. Velocity increases with the membrane length because of continuous water transfer to the gas phase. As it is seen, the model considers the effect of entrance on the hydrodynamics of fluid flow in the gas side.

3.5. Effect of water inlet velocity

Influence of water velocity on evaporation flux of water in membrane module is shown in Fig. 8. As it is seen, increase of water inlet velocity enhances evaporation flux. This observation could be attributed to the enhancement of heat transfer by increasing liquid velocity. The latter would result in increment of water vapor flux by liquid-phase velocity.

4. Conclusions

A membrane evaporator was simulated in this work. For simulation of process, a comprehensive mathematical model was developed to predict transport of water through the membrane. The model was based on numerical solution of basic transport phenomena equations in all compartments of membrane evaporator. Finite element method (FEM) was employed to solve the governing equations utilizing CFD technique. The simulation results were validated by comparing with the experimental data for the evaporation of pure water in flat-sheet membrane contactor. Comparisons confirmed good agreement among the model findings and the experimental data for the flux of water evaporation at different gas velocities.

Acknowledgements

Research council of Islamic Azad University, South Tehran Branch, is highly acknowledged for the financial support of this work.

Nomenclature

A	—	surface area, m^2
C	—	concentration, mol/m^3
D	—	diffusion coefficient, m^2/s
k	—	membrane conductivity, W/m^2 K

k_m — mass transfer coefficient, kg/m^2 s
L — length of the membrane, m
M_w — water molecular weight, kg/mol
p_t — total pressure, Pa
p_w^{sat} — saturated vapor pressure, Pa
R_i — overall reaction rate of any species, mol/m^3 s
T — temperature, K
t — time, s
V — velocity in the module, m/s
x — x-coordinate, m
y — y-coordinate, m
z — z-coordinate, m

Greek symbols

τ — tortuosity factor
ε — membrane porosity
η — viscosity, kg/m^2 s

Abbreviations

CFD — computational fluid dynamics
FEM — finite element method
MD — membrane distillation
ME — membrane evaporation
OE — osmotic evaporation

References

[1] E. Drioli, A. Criscuoli, E. Curcio, Membrane Contactors: Fundamentals, Applications and Potentialities, Elsevier, Amsterdam, 2006.
[2] M. Mulder, Basic Principles of Membrane Technology, Kluwer Academic Publishers, Netherlands, 1991.
[3] W. Kunz, A. Benhabiles, R. Ben-Aïm, Osmotic evaporation through macroporous hydrophobic membranes: A survey of current research and applications, J. Membr. Sci. 121 (1996) 25–36.
[4] N. Hengl, A. Mourgues, E. Pomier, M.P. Belleville, D. Paolucci-Jeanjean, J. Sanchez, G. Rios, Study of a new membrane evaporator with a hydrophobic metallic membrane, J. Membr. Sci. 289 (2007) 169–177.
[5] A. Marjani, S. Shirazian, CFD simulation of mass transfer in membrane evaporators for concentration of aqueous solutions, Orient. J. Chem. 28 (2012) 83–87.
[6] S. Shirazian, S.N. Ashrafizadeh, 3D Modeling and simulation of mass transfer in vapor transport through porous membranes, Chem. Eng. Technol. 36 (2013) 177–185.
[7] K.W. Lawson, D.R. Lloyd, Membrane distillation, J. Membr. Sci. 124 (1997) 1–25.
[8] J. Romero, H. Draga, M.P. Belleville, J. Sanchez, C. Combe-James, M. Dornier, G.M. Rios, New hydrophobic membranes for contactor processes—Applications to isothermal concentration of solutions, Desalination 193 (2006) 280–285.
[9] N. Hengl, A. Mourgues, M.P. Belleville, D. Paolucci-Jeanjean, J. Sanchez, Membrane contactor with hydrophobic metallic membranes: 2. Study of operating parameters in membrane evaporation, J. Membr. Sci. 355 (2010) 126–132.
[10] A. Mourgues, N. Hengl, M.P. Belleville, D. Paolucci-Jeanjean, J. Sanchez, Membrane contactor with hydrophobic metallic membranes: 1. Modeling of coupled mass and heat transfers in membrane evaporation, J. Membr. Sci. 355 (2010) 112–125.
[11] E.L. Cussler, Diffusion Mass Transfer in Fluid Systems, Cambridge University Press, New York, NY, 1997.
[12] A. Gabelman, S.T. Hwang, Hollow fiber membrane contactors, J. Membr. Sci. 159 (1999) 61–106.
[13] N.S. Abdullah, D.B. Das, H. Ye, Z.F. Cui, 3D bone tissue growth in hollow fibre membrane bioreactor: Implications of various process parameters on tissue nutrition, Wichtig, Milano, 2006.
[14] H. Ye, D.B. Das, J.T. Triffitt, Z. Cui, Modelling nutrient transport in hollow fibre membrane bioreactors for growing three-dimensional bone tissue, J. Membr. Sci. 272 (2006) 169–178.
[15] N.S. Abdullah, D.B. Das, Modelling nutrient transport in hollow fibre membrane bioreactor for growing bone tissue with consideration of multi-component interactions, Chem. Eng. Sci. 62 (2007) 5821–5839.
[16] M.H. Al-Marzouqi, M.H. El-Naas, S.A.M. Marzouk, M.A. Al-Zarooni, N. Abdullatif, R. Faiz, Modeling of CO_2 absorption in membrane contactors, Sep. Purif. Technol. 59 (2008) 286–293.
[17] S. Shirazian, A. Moghadassi, S. Moradi, Numerical simulation of mass transfer in gas–liquid hollow fiber membrane contactors for laminar flow conditions, Simul. Modell. Pract. Theory 17 (2009) 708–718.
[18] S. Shirazian, S.N. Ashrafizadeh, Mass transfer simulation of caffeine extraction by subcritical CO_2 in a hollow-fiber membrane contactor, Solvent Extr. Ion Exch. 28 (2010) 267–286.
[19] S. Shirazian, S.N. Ashrafizadeh, Mass transfer simulation of carbon dioxide absorption in a hollow-fiber membrane contactor, Sep. Sci. Technol. 45 (2010) 515–524.
[20] M. Hemmati, N. Nazari, A. Hemmati, S. Shirazian, Phenol removal from wastewater by means of nanoporous membrane contactors, J. Ind. Eng. Chem. 21 (2015) 1410–1416.
[21] M. Ghadiri, S. Fakhri, S. Shirazian, Modeling of water transport through nanopores of membranes in direct-contact membrane distillation process, Poly. Eng. Sci. 54 (2014) 660–666.
[22] S.A. Miramini, S. Razavi, M. Ghadiri, S.Z. Mahdavi, S. Moradi, CFD simulation of acetone separation from an aqueous solution using supercritical fluid in a hollow-fiber membrane contactor, Chem. Eng Process. 72 (2013) 130–136.
[23] F. Nosratinia, M. Ghadiri, H. Ghahremani, Mathematical modeling and numerical simulation of ammonia removal from wastewaters using membrane contactors, J. Ind. Eng. Chem. 20 (2014) 2958–2963.
[24] F. Barati, M. Ghadiri, R. Ghasemi, H.M. Nobari, CFD simulation and modeling of membrane-assisted separation of organic compounds from wastewater, Chem. Eng. Tech. 37 (2014) 81–86.
[25] F. Fadaei, V. Hoshyargar, S. Shirazian, S.N. Ashrafizadeh, Mass transfer simulation of ion separation by nanofiltration considering electrical and dielectrical effects, Desalination 284 (2012) 316–323.
[26] F. Fadaei, S. Shirazian, S.N. Ashrafizadeh, Mass transfer simulation of solvent extraction in hollow-fiber membrane contactors, Desalination 275 (2011) 126–132.

[27] F. Fadaei, S. Shirazian, S.N. Ashrafizadeh, Mass transfer modeling of ion transport through nanoporous media, Desalination 281 (2011) 325–333.
[28] M. Ghadiri, A. Marjani, S. Shirazian, Mathematical modeling and simulation of CO_2 stripping from monoethanolamine solution using nano porous membrane contactors, Int. J. Greenhouse Gas Control 13 (2013) 1–8.
[29] M. Ghadiri, S. Shirazian, Computational simulation of mass transfer in extraction of alkali metals by means of nanoporous membrane extractors, Chem. Eng. Process. 69 (2013) 57–62.
[30] A. Marjani, S. Shirazian, Simulation of heavy metal extraction in membrane contactors using computational fluid dynamics, Desalination 281 (2011) 422–428.
[31] S.M.R. Razavi, S.M.J. Razavi, T. Miri, S. Shirazian, CFD simulation of CO_2 capture from gas mixtures in nanoporous membranes by solution of 2-amino-2-methyl-1-propanol and piperazine, Int. J. Greenhouse Gas Control 15 (2013) 142–149.
[32] M. Rezakazemi, Z. Niazi, M. Mirfendereski, S. Shirazian, T. Mohammadi, A. Pak, CFD simulation of natural gas sweetening in a gas–liquid hollow-fiber membrane contactor, Chem. Eng. J. 168 (2011) 1217–1226.
[33] M. Rezakazemi, M. Shahverdi, S. Shirazian, T. Mohammadi, A. Pak, CFD simulation of water removal from water/ethylene glycol mixtures by pervaporation, Chem. Eng. J. 168 (2011) 60–67.
[34] M. Rezakazemi, S. Shirazian, S.N. Ashrafizadeh, Simulation of ammonia removal from industrial wastewater streams by means of a hollow-fiber membrane contactor, Desalination 285 (2012) 383–392.
[35] S. Shirazian, A. Marjani, F. Fadaei, Supercritical extraction of organic solutes from aqueous solutions by means of membrane contactors: CFD simulation, Desalination 277 (2011) 135–140.